

Nonlinear optics in gallium phosphide cavities: simultaneous second and third harmonic generation

Blaine McLaughlin¹, David P. Lake^{2,1}, Matthew Mitchell^{3,1}, and Paul E. Barclay^{1,*}

¹Department of Physics and Astronomy and Institute for Quantum Science and Technology, University of Calgary, Calgary, AB, T2N 1N4, Canada

²Department of Applied Physics & Materials Science, California Institute of Technology, Pasadena, CA, 91125, United States

³Stewart Blusson Quantum Matter Institute, University of British Columbia, Vancouver, BC, V6T 1Z4, Canada

*Corresponding author: pbarclay@ucalgary.ca

July 8, 2022

Abstract

We demonstrate the simultaneous generation of second and third harmonic signals from a telecom wavelength pump in a gallium phosphide (GaP) microdisk. Using analysis of the power scaling of both the second and third harmonic outputs and calculations of nonlinear cavity mode coupling factors, we study contributions to the third harmonic signal from direct and cascaded sum frequency generation processes. We find that despite the relatively high material absorption in gallium phosphide at the third harmonic wavelength, both of these processes can be significant, with relative magnitudes that depend closely on the detuning between the second harmonic wavelength of the cavity modes.

1 Introduction

In recent years, resonant cavity structures have been used in a wide range of applications within integrated photonics. In particular, whispering gallery mode microcavities have allowed for the incorporation of non-

linear optical effects into on-chip photonics platforms [25]. The high degree of optical confinement provided by whispering gallery mode microcavities allows for integrated nonlinear devices with great efficiency and a high degree of control over the nonlinear behavior. For example, nonlinear phenomena such as second harmonic generation (SHG), sum frequency generation (SFG), third harmonic generation (THG) and Kerr frequency comb generation have been realized in lithium niobate (LN) [6, 35, 31, 27, 30, 9, 58, 11, 8, 7], SiN [23, 37, 41], AlN [40, 4, 16], GaN [46, 34], GaAs [19], GaP [43, 44, 28, 22, 48, 55], and AlN/SiN composite [51] microcavities.

Many nonlinear photonic devices are designed for the optimization of a specific nonlinear process. However, nonlinear photonic materials often possess significant optical nonlinearities in both the second and third order. While unwanted nonlinear effects of a given order can be minimized through device design, for sufficiently large nonlinearities, both second and third-order processes contribute to a device's response. In particular, generation of the third harmonic may occur due to competing second- and third-order nonlinear processes [25]: the process of cas-

caded sum frequency generation (CSFG), a second-order nonlinear process that can produce a third harmonic, occurs independently of direct third harmonic generation (DTHG). These competing processes and their efficiencies will in general depend on the relative strengths of the material’s nonlinear susceptibilities and the device’s optical mode spectrum. A device could be designed with parameters to optimize the generation of one process over another following the theory in reference [25]. However, in a non-optimized device the contributions from each harmonic generation process may not be immediately obvious. It is therefore necessary to develop experimental methodology for discerning the contributions from each process to the third harmonic signal.

Generation of simultaneous SH and TH signals has previously been observed in LN [27, 26], Mg:LN [47], and GaP [48] microcavities. However, in these cases the third harmonic generation process is assumed to be either CSFG (in LN) or DTHG (in GaP). A detailed study of the generation processes of third harmonic signals in these devices has not yet been performed. Here we demonstrate the simultaneous observation of SH and TH signals generated from a telecom pump in a GaP microdisk cavity and measure their dependence on pump power and wavelength. These harmonic signals can be attributed, respectively, to a quasi-phase matched (QPM) SHG, and both DTHG and a QPM CSFG processes. The presence of CSFG is indicated by a saturation of the SH signal at high input power. Through use of coupled-mode theory, we predict that the third harmonic output power from CSFG and DTHG will scale differently with the coupled first harmonic input power. Additional analysis was performed with finite-difference time-domain (FDTD) simulations. Using the simulated whispering gallery modes (WGMs) of our microdisk devices, we calculate the nonlinear mode coupling factors that dictate the strength of the nonlinear mode interactions, and find that they are consistent with experimentally observed behaviour.

We begin in Section 2 by theoretically analysing the nonlinear harmonic generation processes in gallium phosphide microdisks. In Section 3 we use this theory to analyse experimentally observed SH and

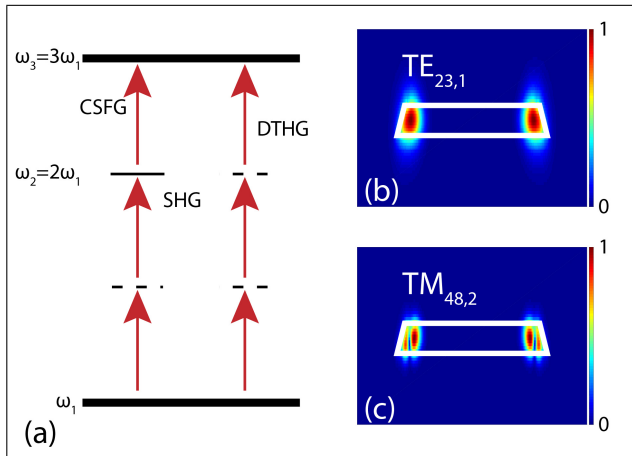


Figure 1: (a) Energy level diagram of the SHG, CSFG and THG processes. Solid lines indicate WGM resonant modes, while dashed lines represent virtual energy levels. (b) Image of FDTD simulated field magnitude of the TE_{23,1} microdisk mode. (c) Image of FDTD simulated normalized absolute field magnitude of the TM_{48,2} microdisk mode.

TH signals from a gallium phosphide microdisk. In Section 4 we compare these results with theory, and discuss future improvements for enhancing SH and TH processes in these devices.

2 Theory of harmonic generation in microdisks

The GaP microdisk devices used in this experiment were fabricated following the process in Ref. [33]. The device under study has a radius of 3.05 μm and a thickness of 250 nm, with a sidewall angle of 70° resulting from the fabrication process. Previous experiments using these devices include observation of optomechanical coupling [33] and SHG from telecommunication to near-IR wavelengths [22]. During the SHG experiments, an additional signal corresponding to a third harmonic was also observed, but not studied in detail. A similar TH signal was observed but not studied in detail in an independent experiment with GaP photonic crystals by Schneider et al. [48].

The presence of simultaneous SH and TH generation indicates that despite higher loss due to material absorption in GaP at the green TH wavelength, wavelength conversion with sufficiently high efficiency is still possible. However, we can not naively assume that one of CSFG or DTHG is the process primarily responsible.

Figure 1a shows an example energy diagram of the possible harmonic generation processes. Light at frequency ω_0 is coupled from a waveguide into a microdisk supporting a mode with frequency ω_1 close to ω_0 . Efficient nonlinear wave mixing processes can occur when the cavity also supports higher frequency modes whose frequencies are near the harmonics of the fundamental mode at ω_1 . We consider a device with modes at frequencies $\omega_2 \approx 2\omega_1$ and $\omega_3 \approx 3\omega_1$. While the excitation of photons from ω_1 to ω_2 will dominantly occur through SHG, excitation to ω_3 can occur through two processes. The direct third-order process, DTHG, occurs independently of the SHG process assuming that we are operating with an undepleted pump. Conversely, excitation to ω_3 through CSFG is an entirely second-order nonlinear process, where light from the first and SH modes undergoes sum frequency generation (SFG) to excite the TH mode. In a material with a weak third-order nonlinear susceptibility, observed TH signals can be predominantly from CSFG [26]. In a material with both strong second- and third-order susceptibilities, both processes can contribute significantly.

In a microcavity fabricated from a crystalline material, harmonic generation processes between modes are restricted due to polarization and phase matching requirements. The electric field of a TE(TM)-like WGM mode is given by $\mathbf{E}_{\text{TE(TM)}_{m,n}}(r, \varphi, z) \sim \mathbf{e}_{\text{TE(TM)}_{n,m}}(r, z) \exp(im\varphi)$, where n and m are the radial and azimuthal mode orders respectively. $\mathbf{e}_{\text{TE(TM)}} is the two-dimensional cross section of the field in the rz -plane. The free spectral range of microdisk devices here vary with n , as previously demonstrated in previous devices [33]. The fundamental TE mode in the 1550 nm range has a free spectral range of 40 nm. Higher order modes have larger free spectral range. We assume that the WGM modes in our structure with higher-order vertical in-$

dex can be ignored, which is valid whenever the device is sufficiently thin [2]. The modes of a microdisk differ from the perfectly polarized TE or TM modes of a cylindrical cavity [14]; rather they contain non-zero field components for all dimensions, with the in-plane (i.e. \hat{r}) component resembling a typical TE field, and the out-of-plane component (i.e. \hat{z}) resembling a typical TM field. We use the polarization notation of Borselli [2], where a mode whose largest components are in-plane are considered 'TE-like', and modes whose largest components are out-of-plane are 'TM-like'. Figures 1b and 1c respectively show the simulated cross-sectional profile of the absolute value $|\mathbf{E}|$ of the $\text{TE}_{23,1}$ and $\text{TM}_{48,2}$ microdisk modes for the device studied here.

In the case of a cavity with cylindrical symmetry, the phase matching conditions of a nonlinear process can be expressed in terms of the azimuthal indices m [20]. Additional angular momentum quanta are accumulated due to the Berry phase of the WGM orbiting the cavity [53], whose amount depends on the symmetry of the cavity material's crystal lattice [29]. GaP possesses $\bar{4}3m$ symmetry, with the crystal axis inverting with a $\pi/2$ rotation. The second-order susceptibility components will change sign under this transformation, while the third-order susceptibility components remain unchanged. As such, there is an additional factor of $\Delta m = \pm 2$ added to all second-order phase matching requirements, while the third-order phase matching requirements remain unchanged. The quasi-phase matching conditions for SHG, CSFG and DTHG in GaP are therefore:

$$\text{SHG} : m_2 = 2m_1 \pm 2, \quad (1)$$

$$\text{CSFG} : m_3 = m_1 + m_2 \pm 2, \quad (2)$$

$$\text{DTHG} : m_3 = 3m_1. \quad (3)$$

In principle, it is possible for a given set of modes with azimuthal orders $\{m_1, m_2, m_3\}$ to satisfy all three phase matching processes at once, leading to a TH signal generated both directly through phase matched DTHG and indirectly through $\bar{4}$ -quasi-phase matched CSFG.

2.1 Coupled Mode Theory

For nonlinear materials, the dependence of the nonlinear polarization on the electric field leads to a self-referencing wave equation [3], in which the electric field strength of the higher harmonic frequency modes depends directly on the field strength at the input fundamental frequency mode. This dependence can be expressed as a set of steady-state equations giving the field amplitudes of each optical mode in the microdisk as functions of the other optical mode amplitudes, as well as the field of the input coupling waveguide. The amplitude equation for a standing-wave mode in a waveguide coupled cavity of generic mode index k is [10, 45, 24, 32, 21]:

$$\frac{d}{dt}a_k = \left(i\omega_k - \frac{\kappa_k}{2}\right)a_k + \sqrt{\frac{\kappa_{k,ex}}{2}}s_+, \quad (4)$$

with the waveguide transmission given by

$$s_- = s_+ - \sqrt{\frac{\kappa_{k,ex}}{2}}a_k, \quad (5)$$

where a_k is the electric field mode amplitude of the cavity, $s_{+(-)}$ is the incoming (outgoing) waveguide field amplitude flux, ω_k is the mode frequency and κ_k is the mode energy decay rate. The quality factor of a mode is defined here as $Q_k \equiv \omega_k/\kappa_k$. κ_k can be separated into contributing components

$$\kappa_k = \kappa_{k,i+p} + \kappa_{k,ex}. \quad (6)$$

Here $\kappa_{k,i+p}$ is the intrinsic plus parasitic energy decay rate of the cavity, understood as the rate of energy loss into all channels other than the output mode of the waveguide, including radiation loss, optical absorption, and coupling to lossy higher-order waveguide modes [50]. $\kappa_{k,ex}$ is the external energy decay rate due to the coupling between the cavity and the fundamental waveguide mode, which is used as the input and output mode. The field amplitudes are normalized such that $|a_k|^2$ is the circulating mode energy and $|s_{\pm}|^2$ is the incoming (outgoing) power flow through the waveguide. From (2), the outgoing power output from the cavity mode k is $P_k = (\kappa_{k,ex}/2)|a_k|^2$.

To model our microdisk system, we consider a set of nearly triply resonant modes at frequencies $\omega_{1,2,3}$.

The waveguide input s_+ is set to be nearly resonant with the fundamental mode: $\omega_0 \approx \omega_1$. Due to nonlinear effects, it can couple to the SH and TH cavity modes. Following the analyses of Rodriguez et al. [45] and Li et al. [24], we obtain a set of coupled mode equations,

$$\frac{d}{dt}a_1 = \left(i\omega_1 - \frac{\kappa_1}{2}\right)a_1 + \sqrt{\frac{\kappa_{1,ex}}{2}}s_+, \quad (7)$$

$$\frac{d}{dt}a_2 = \left(i\omega_2 - \frac{\kappa_2}{2}\right)a_2 - i\omega_2\beta_{\text{CSFG}}a_1^*a_3 + i\omega_2\beta_{\text{SHG}}a_1^2, \quad (8)$$

$$\frac{d}{dt}a_3 = \left(i\omega_3 - \frac{\kappa_3}{2}\right)a_3 + i\omega_3\beta_{\text{CSFG}}^*a_1a_2 + i\omega_3\beta_{\text{DTHG}}a_1^3, \quad (9)$$

where $\beta_{\text{SHG,CSFG,DTHG}}$ are the inter-modal coupling factors associated with each nonlinear frequency conversion process. For second-order nonlinear processes, the coupling factors have dimensions of $J^{-1/2}$, while for third-order nonlinear processes, the coupling factors have dimensions of J^{-1} . The individual terms in these equations can be understood as corresponding to photon creation for each a_k term and photon annihilation for each a_k^* term. We apply an undepleted-pump approximation, where the loss in the first harmonic mode due to the harmonic generation processes is considered negligible. This assumption is valid for low input powers on the order of ~ 1 mW [24].

Applying the rotating-wave approximation for each equation and solving for the steady state gives the harmonic mode output powers:

$$P_2 = \frac{\eta_{\text{SHG}}P_{in}^2}{(1 + \zeta P_{in})^2}, \quad (10)$$

$$P_3 = \eta_{\text{DTHG}}P_{in}^3 + \frac{\eta_{\text{CSFG}}P_{in}^3}{(1 + \zeta P_{in})^2}, \quad (11)$$

where $\eta_{\text{SHG,CSFG,DTHG}}$ is the conversion efficiency of each harmonic generation process, and ζ is a power saturation term which arises due to the CSFG process. In the special case of a triple resonance, i.e. $\Delta_1 = \Delta_2 = \Delta_3 = 0$ (where $\Delta_k = \omega_k - k\omega_0$, $k \in 1, 2, 3$ is the frequency detuning of the resonant microdisk mode from the harmonic frequency $k\omega_0$), the efficien-

cies and saturation parameter are given by:

$$\eta_{\text{SHG}} = 32\omega_1^2 |\beta_{\text{SHG}}|^2 \frac{\kappa_{1,ex}^2 \kappa_{2,ex}}{\kappa_1^4 \kappa_2^2}, \quad (12a)$$

$$\eta_{\text{DTHG}} = 144\omega_1^2 |\beta_{\text{DTHG}}|^2 \frac{\kappa_{1,ex}^3 \kappa_{3,ex}}{\kappa_1^6 \kappa_3^2}, \quad (12b)$$

$$\eta_{\text{CSFG}} = 2304\omega_1^4 |\beta_{\text{SHG}}|^2 |\beta_{\text{CSFG}}|^2 \frac{\kappa_{1,ex}^3 \kappa_{3,ex}}{\kappa_1^6 \kappa_2^2 \kappa_3^2}, \quad (12c)$$

$$\zeta = 96\omega_1^2 |\beta_{\text{CSFG}}|^2 \frac{\kappa_{1,ex}}{\kappa_1^2 \kappa_2 \kappa_3}, \quad (12d)$$

where the β terms are mode coupling factors discussed in detail below. For low powers, the SH and TH outputs scale approximately quadratically and cubically respectively, consistent with the power scaling from pure SHG and THG. At higher input powers, the SFG process begins to deplete the SH mode energy, in a manner that scales quadratically with pump power.

2.2 Nonlinear Mode Coupling Factors

Here we provide an analysis of the nonlinear coupling factors β_{SHG} , β_{CSFG} , β_{DTHG} , their dependence on the field profiles of the phase-matched modes, and their effects on the overall harmonic generation processes. The magnitudes of the coupling factors are determined by the spatial overlap of the fields of each mode participating in a given process. Following the analysis of Rodriquez et al. [45], we derive an expression for the small change in the frequency of a given microdisk mode due to nonlinear polarization. When the perturbed mode frequencies are introduced into (4), we will obtain the coupled mode Eqs. (7-9) with explicit expressions for the coupling factors.

We consider a perturbation of the microdisk's dielectric constant $\delta\varepsilon$ resulting from a nonlinear optical polarization $\delta\mathbf{P} = \delta\varepsilon\mathbf{E}$. The corresponding fractional change in the mode frequency is proportional to the fraction of electric field energy in the perturbation [15]:

$$\frac{\delta\omega_k}{\omega_k} = -\frac{1}{2} \frac{\int_{\varepsilon} \mathbf{E}^* \cdot \delta\mathbf{P}_k d^3\mathbf{x}}{\int \varepsilon |\mathbf{E}|^2 d^3\mathbf{x}}, \quad (13)$$

where \mathbf{E} is the unperturbed electric field. Substituting $\omega_k \rightarrow \omega_k + \delta\omega_k$ into (4) for each mode $k = 1, 2, 3$

and rearranging for terms proportional to a_k then reproduces Eqs. (7-9) with explicit expressions for each β term given in terms of the field integrals. In order to maintain the mode amplitude normalization where $|a_k|^2$ is in units of energy, it is necessary to apply an additional normalization term $(\int \varepsilon |\mathbf{E}_k|^2 d^3\mathbf{x})^{1/2}$ to each β term for each \mathbf{E}_k in the numerator. This gives the nonlinear coupling factors:

$$\beta_{\text{SHG}} = \frac{1}{4} \frac{\int d^3\mathbf{x} \sum_{ijk} \varepsilon \chi_{ijk}^{(2)} [E_{1i}^* E_{2j} E_{1k}^* + E_{1i}^* E_{1j}^* E_{2k}]}{\int d^3\mathbf{x} \varepsilon |E_1|^2 (\int d^3\mathbf{x} \varepsilon |E_2|^2)^{1/2}}, \quad (14)$$

$$\beta_{\text{CSFG}} = \frac{1}{4} \frac{\int d^3\mathbf{x} \sum_{ijk} \varepsilon \chi_{ijk}^{(2)} [E_{2i}^* E_{3j} E_{1k}^* + E_{2i}^* E_{1j}^* E_{3k}]}{(\int d^3\mathbf{x} \varepsilon |E_1|^2)^{1/2} (\int d^3\mathbf{x} \varepsilon |E_2|^2)^{1/2} (\int d^3\mathbf{x} \varepsilon |E_3|^2)^{1/2}}, \quad (15)$$

$$\beta_{\text{DTHG}} = \frac{3}{8} \frac{\int d^3\mathbf{x} \varepsilon \chi^{(3)} (\mathbf{E}_1^* \cdot \mathbf{E}_1) (\mathbf{E}_1^* \cdot \mathbf{E}_3)}{(\int d^3\mathbf{x} \varepsilon |E_1|^2)^{1/2} (\int d^3\mathbf{x} \varepsilon |E_3|^2)^{3/2}}, \quad (16)$$

where $\chi^{(2)}$ and $\chi^{(3)}$ are the second- and third-order nonlinear electric susceptibilities respectively, and $\{i, j, k\}$ label the \hat{x} , \hat{y} and \hat{z} components of \mathbf{E} . The coupling factors can be further simplified depending on the symmetries of the device, as well as the symmetries of the nonlinear susceptibility tensors.

To estimate the values of the nonlinear coupling factors in the experiment, we have calculated the coupling factors of several potential combinations of modes obtained from FDTD simulations (performed using MEEP [38]) of WGMs in our microdisk. The cylindrical symmetry of the microdisk allows us to specify the azimuthal mode number m in the simulations. We identify the $\text{TE}_{23,1}$ mode to be closest fundamental mode to the target pump wavelength of 1557 nm (190 THz) used in the experiment presented below. Figure 1b shows the normalized absolute field profile of this mode. For crystals such as GaP with $\bar{4}3m$ symmetry, a TE pump field undergoing harmonic generation processes must produce a TM-like SH mode, and a TE-like TH mode [3]. Additionally, SFG between a TE and a TM mode must produce a TE mode. Several TM and TE modes near the target SH and TH frequencies were simulated for phase matched azimuthal mode numbers and several radial mode numbers. Only the lowest vertical order

TE and TM microdisk modes were considered in our calculations. Our simulations use a value of $n = 3.01$ for all modes. Since the refractive index of GaP is dispersive in the visible regime [39], there is considerable uncertainty in the simulated higher harmonic mode frequencies. The resulting field profiles were substituted into Eqs. (14), (15) and (16) to calculate the coupling factors. Note that in general, energy matching ($\omega_2 = 2\omega_1$ etc.) is not always satisfied for a given combination of modes due to dispersion of the microdisk and GaP material. However, these calculations shed insight into relative strengths of the various coupling processes. Energy conservation is taken into account below when identifying candidate mode combinations.

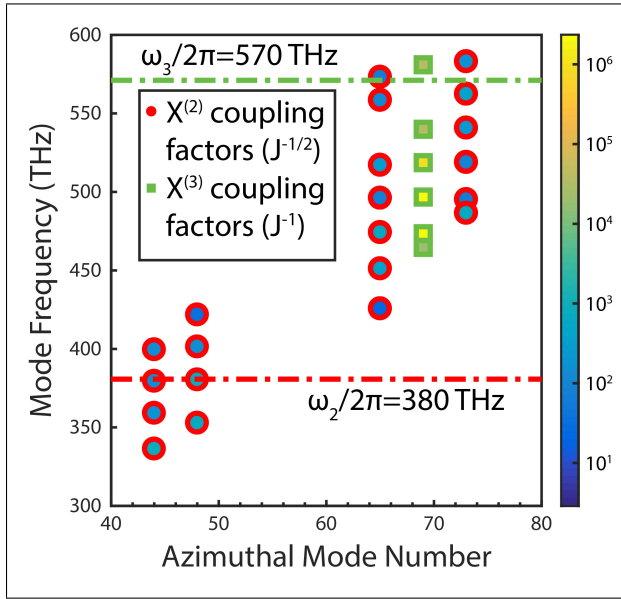


Figure 2: Absolute values of second-order (outlined in red circles) and third-order (outlined in green squares) nonlinear coupling factors with the $TE_{23,1}$ first harmonic mode. Groups of phase matched microdisk modes are plotted by the frequency and azimuthal number of the highest harmonic mode in the wave mixing process.

Figure 2 shows the resulting calculated coupling factors for the $TE_{23,1}$ first harmonic mode. The

mode combinations are grouped into coupling factors corresponding to second-order (highlighted in red) and third-order (highlighted in green) conversion processes. β values are plotted in units of $J^{-1/2}$ for second-order processes and J^{-1} for third-order processes, following the conventions of previous works on second and third-order harmonic generation processes in microresonators [45, 28]. We obtain coupling factors on the order of $1 \sim 100 J^{-1/2}$ for $\beta_{SHG,CSFG}$ and $10^4 \sim 10^6 J^{-1}$ for β_{DTHG} . Dashed lines corresponding to the SH and TH frequencies (around 380 and 570 THz) are provided to highlight which mode combinations conserve energy. Efficient harmonic generation is predicted to occur for phase matched microdisk modes with small detunings from the harmonic frequencies.

Although it can be difficult to precisely identify which mode coupling processes are responsible for observed SH and TH signals, the magnitudes of the nonlinear coupling factors provide useful information on the relative efficiencies of the DTHG and CSFG processes. This is most useful at low input powers, where the contributions from DTHG and CSFG processes cannot be determined from power scaling. One can define a critical SH quality factor $Q_{2,c} = \frac{1}{2} |\beta_{DTHG}| / (|\beta_{SHG}| + |\beta_{CSFG}|)$ following the method in Ref. [24], which dictates the condition for which both processes are equally efficient. This is obtained from setting the ratio of Eqs. (12b) and (12c) to unity. DTHG typically dominates the THG process for mode combinations with $Q_2 \ll Q_{2,c}$, and likewise CSFG dominates for $Q_2 \gg Q_{2,c}$. From our coupling factor calculations, values of $Q_{2,c}$ for mode combinations that are phase matched for both DTHG and CSFG vary between $1 \sim 10^3$. Considering that previous measurements of our devices show $Q \sim 10^4$ close to the SH wavelength of 778 nm [22], these results suggest that CSFG is more likely to dominate in our devices in the ideal scenario of zero detuning. However, for non-zero Δ_2 , $Q_{2,c}$ is reduced following the Lorentzian lineshape of the SH mode, and as we will find experimentally below, DTHG can become more significant. Note that $Q_{2,c}$ is only well defined in the case that the third harmonic mode satisfies the phase matching conditions for both CSFG and

DTHG. In the case where the third harmonic mode is phase matched to only one of DTHG or CSFG, we expect that only the phase matched process may occur.

3 Experiment

To observe SH and TH signals from GaP microdisks, we used a similar setup as in our previous studies of SHG in these devices [22]. A fiber taper waveguide is used to evanescently couple light into microdisk modes, and to collect the SH and TH output. A continuous wave tunable laser (New Focus TLB-6700) with a central wavelength around 1557 nm was input to high- Q microdisk resonances. Most high- Q modes of the devices were found to exhibit SH signals, as in Ref. [22]. During these previous SHG studies, some modes were also observed to generate TH signal. Here we study a microdisk supporting a mode whose TH output was largest among measured devices, suggesting the presence of a microdisk mode close to resonance with the TH frequency. However, additional resonant spectroscopy measurements are required to confirm its precise detuning.

We perform a wavelength sweep over the pump resonance for various input powers within the range of 1-10 mW, where the saturation effects of CSFG are predicted to begin to occur [24]. In order to minimize heating and photothermal dispersion of the microdisk mode wavelengths [5], the pump field amplitude was modulated with an electro-optic modulator (EOM) controlled by a waveform generator (Stanford DG535) outputting a square wave signal with a duty cycle of 0.5%. The pump wavelength was independently measured using an optical spectrum analyzer (ANDO AQ6137B). The pump was then sent through an erbium-doped fiber amplifier (PriTel LNHP-FA-27-IO-CP). A variable optical attenuator (EXFO FVA-3100) was used to set the power input to the fiber taper. A set of polarization controllers were set to maximise coupling between the fiber taper field and microdisk resonances of interest. A 90:10 beamsplitter sent 10% of the fiber taper output to a power meter (Newport 1936-R) for measuring the pump transmission, and 90% to a spectrometer

(Princeton Instruments SP2750 and Excelon PIXIS 100B CCD array). Because of the difference in power outputs at the SH and TH wavelengths, it was necessary to conduct the experiment in two sets, one for each harmonic signal. The SH signal saturated the spectrometer CCD for the input powers used here. Therefore, a neutral density filter was used at the spectrometer input to attenuate it. No such attenuation of the TH signal was required.

Figure 3a shows the transmission of the fiber taper when the pump wavelength is scanned over the first harmonic resonance for a 8.7 mW input power. A Fano lineshape was observed due the fiber taper touching the edge of the microdisk. This positioning stabilizes the fiber taper and maximizes coupling to the TH output, however, it also enhances coupling to higher-order modes of the fiber taper, resulting in a non-Lorentzian resonance lineshape [56]. From fits to the Fano lineshapes, we obtain the pump mode decay rates $\kappa_1 = 2.0 \times 10^{10}$ rad/s and $\kappa_{1,ex} = 3.5 \times 10^9$ rad/s, corresponding to $Q_1 \sim 6 \times 10^4$. Due to a lack of suitable tunable lasers, we were unable to directly measure the SH and TH mode spectra.

Figures 3b and 3c show the measured SH and TH output powers from the fiber taper, respectively, as a function of varying pump wavelength for several input powers. The corresponding wavelengths of the peak SH and TH signal are plotted on the top x -axis as a reference. From this we see that the SH and TH signals are enhanced when the pump is resonant with the cavity mode, as expected. Here the input power is defined by the power in the fiber taper immediately before the coupling region. Each point in the data set is extracted from the measured spectra of each harmonic at a given input power and finely tuned pump wavelength. A Gaussian lineshape was fit to the spectrometer resolution limited harmonic spectra, and the total number of spectrometer CCD counts under each lineshape were converted to fiber taper output power, taking into account the various efficiencies and losses of the experimental apparatus. While we attempted to limit photothermal dispersion through pulse modulation, we still observe a wavelength drift in the second harmonic spectra that increases with increasing pump power, behaving in correspondence with photothermal dispersion effects [5].

The fringed dependence of the SH power on pump wavelength is related to etaloning effects in the system, which are common in back illuminated CCD detectors at near-infrared wavelengths [13].

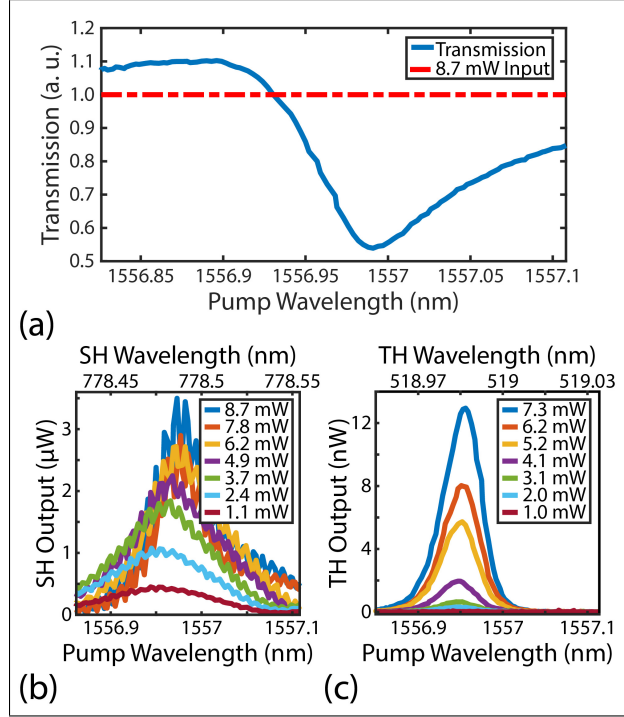


Figure 3: (a) Transmission spectrum of GaP microdisk pump mode around 1557 nm for a 8.7 mW pump power. The Fano-like lineshape of the observed resonance is attributed to a phase mismatch between the coupled fiber taper modes. (b) Second and (c) third harmonic output signal power for several pump wavelengths and input powers. Top axes show the observed peak harmonic wavelength measured in the spectrometer.

Figure 4 plots the peak SH (orange) and TH (green) output powers as a function of pump power. The solid lines are fits to the SH and TH outputs using Eqs. (10) and (11). This data shows that the peak SH output power scales sub-quadratically with the input power, with the slope decreasing with increasing input power, indicating a saturation of the SH signal due to CSFG predicted by the denominator of (10).

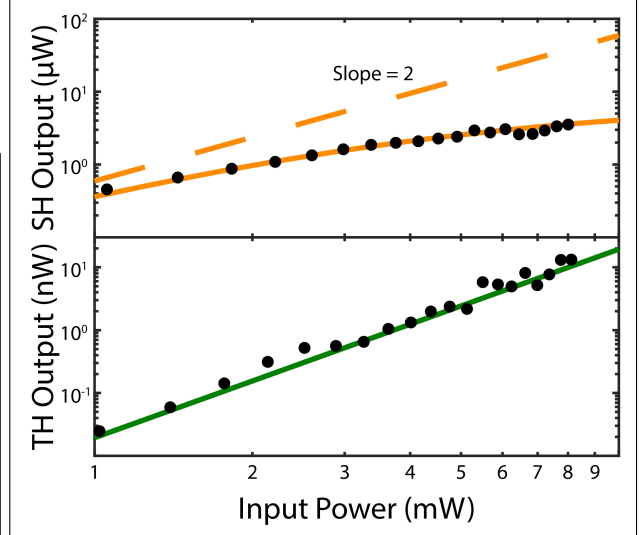


Figure 4: On-resonance output power for second (orange) and third harmonic (green) signals. Solid lines are fits to the saturated resonance theory. The dashed line corresponds to quadratic power scaling predicted from zero depletion.

The peak TH signal is approximately cubic with respect to the input power over the measured range, with a corresponding slope approximately equal to 3 on a log scale.

The lack of sub-cubic saturation behaviour in our measured TH signal suggests that the DTHG term in (11) is the main THG process in our measurements. However, this disagrees with our earlier theoretical prediction from $Q_{2,c}$ for $\Delta_2 = 0$ that CSFG should dominate. Note that pump depletion would affect both the SHG and THG signals and does not explain the observed behavior [59]. A plausible explanation of the difference in saturation behavior of the SHG and THG signals is that our system possesses non-zero Δ_2 and small Δ_3 . Setting $\eta_{\text{DTHG}} = \eta_{\text{CSFG}}$ for the general case of non-zero Δ_2 and Δ_3 gives the condition $(Q_{2,c}/Q_2)^2((\Delta_2/\kappa_2)^2 + 1) = 1$. Assuming coupling to modes with $Q_{2,c} \sim 10^3$ predicted by our coupling factor calculations, then for $Q_2 \sim 10^4$, the $\eta_{\text{DTHG}}/\eta_{\text{CSFG}} \sim 1$ condition is satisfied when $|\Delta_2| \sim 10\kappa_2$. This value of $|\Delta_2|$ is reduced for

larger $Q_{2,c}$ or smaller Q_2 . If we assume $\Delta_3 \sim 0$, then even with $\Delta_2 \sim 10\kappa_2$ the saturation parameter $\zeta \sim 10 - 20 \text{ \% mW}^{-1}$ depending on the values of $|\beta_{\text{CSFG}}|$ and κ_2 . As shown below, this is consistent with ζ inferred from the measured saturation of the SHG signal.

From our fits, we obtain efficiency and saturation parameters with standard errors of $\eta_{\text{SHG}} = 5.9 (1.6) \times 10^{-2} \text{ \% mW}^{-1}$, $\zeta = 28 (7) \text{ \% mW}^{-1}$, and $\eta_{\text{THG}} = 1.9 (0.1) \times 10^{-6} \text{ \% mW}^{-2}$. Our measured SHG external efficiency is of similar magnitude to what was achieved in previous SHG experiments with different microdisks on the same chip [22]. Our SHG and THG external efficiencies are comparable to or exceed results from similar experiments in LN and MgO:LN microdisk devices [27, 47], but are smaller than current state of the art SHG-THG generation in LN microdisks [26]. However, these LN devices possess $Q \sim 10^5 - 10^6$, larger than our devices. As discussed below, more efficient SHG and THG in GaP devices could be realized by reducing their optical loss, optimizing mode detunings, and improving the microdisk-waveguide output coupling efficiency.

4 Discussion

The GaP microdisks used in this experiment allow simultaneous observation of SHG and THG for relatively low powers. Our observed efficiencies and saturation are limited primarily by detuning from the SH mode, poor coupling between the SH and TH modes and the fundamental fiber taper mode, and material absorption at the TH wavelength. The fiber taper diameter is on the order of $1 \mu\text{m}$ and provides good coupling efficiency at the pump wavelength. However, at the SHG and THG wavelengths, the coupling efficiency is reduced due to lower modal overlap of the fiber taper and microdisks fields, and the multi-mode nature of the fiber taper at these wavelengths. This suggests that the internal CSFG and DTHG conversion efficiencies are larger than what is measured in this work, resulting in a sub-quadratic scaling in the SH signal despite a low TH output power. The TH wavelength of 519 nm lies just outside the transparency window of GaP, leading to ma-

terial absorption. We therefore have a fundamental lower limit on $\kappa_{3,i}$ (i.e. an upper limit on Q_3) due to absorption. The upper limit of the intrinsic quality factor of a cavity at wavelength λ can be approximated as $Q_{i,\text{max}}(\lambda) \approx (2\pi n(\lambda))/(\lambda\alpha(\lambda))$ [36]. Using an attenuation coefficient $\alpha_{\text{GaP}}(519 \text{ nm}) \approx 252 \text{ cm}^{-1}$ [1, 57], we obtain $Q_{3,i,\text{max}} \approx 1700$ or minimum decay rate $\kappa_{3,i,\text{min}} \approx 2.1 \times 10^{12} \text{ rad/s}$.

Using the maximum value of Q_3 predicted above, and assuming $Q_2 \sim 1.0 \times 10^4$, as previously measured in our GaP microdisks [22], for $\Delta_2 \sim \kappa_2$ and $\Delta_3 \sim 0$, we predict from Eqs. (12) efficiency and saturation values on the same order as the measured values for coupling factors of $|\beta_{\text{SHG}}| \sim 10 \text{ J}^{-1/2}$, $|\beta_{\text{CSFG}}| \sim 400 - 500 \text{ J}^{-1/2}$ and $|\beta_{\text{DTHG}}| \sim 2 - 3 \times 10^6 \text{ J}^{-1}$. These coupling factors are on the upper limit of what was calculated for $|\beta_{\text{DTHG}}|$ and $|\beta_{\text{CSFG}}|$, and on the lower limit for $|\beta_{\text{SHG}}|$.

Under ideal conditions for this device, with triple resonance and critical coupling for all harmonic modes, we estimate ideal conversion efficiencies of $\eta_{\text{SHG}} \sim 1.1 \times 10^{-1} \text{ \% mW}^{-1}$, $\eta_{\text{DTHG}} \sim 3.2 \times 10^{-5} \text{ \% mW}^{-2}$, $\eta_{\text{CSFG}} \sim 3.2 \times 10^{-3} \text{ \% mW}^{-2}$, and $\zeta \sim 7.7 \text{ \% mW}^{-1}$ for the coupling factor values listed above. These ideal values for η_{SHG} and η_{CSFG} are an order of magnitude larger than observed in our experiment, suggesting that the measured efficiencies are primarily limited by imperfect mode detuning, as well as undercoupling to the SH and TH modes. The maximum predicted value of η_{DTHG} here is limited by material absorption, and may be enhanced by operating with a pump whose third harmonic wavelength lies within the transparency window of GaP. Additional resonance tuning may be achieved through the use of external temperature control [17, 28] or application of external cladding [52]. The ideal predicted value of ζ is lower than what was measured here, which can be attributed to undercoupling to the SH and TH modes.

In future experiments, both DTHG and CSFG in a GaP microcavity device could be enhanced in several ways. In addition to the techniques mentioned above, optimizations in fabrication processes [12], reductions of sidewall roughness, improvements to waveguide coupling efficiency, dispersion engineer-

ing to ensure triple resonance and maximizing constructive DTHG-CSFG interference [24], and gain-induced loss compensation with dopants [59] would significantly improve the device performance. Alternatively, the use of photonic crystals [42] or topological metamaterials [49, 54, 18] may yield improved performance due to lower mode volumes.

In summary, we have observed the simultaneous generation of SH and TH signals from a telecom pump in GaP microdisks. This work represents the first detailed experimental analysis of third harmonic generation in GaP microcavities. For experiments in which simultaneous second and third generation is observed, the methods presented here will allow systematic analysis of the third harmonic generation processes. Future third harmonic generation experiments in GaP microcavity devices should be performed in carefully designed integrated devices whose modes are optimized for the desired wavelength and power range [24].

© 2022 Optica Publishing Group. One print or electronic copy may be made for personal use only. Systematic reproduction and distribution, duplication of any material in this paper for a fee or for commercial purposes, or modifications of the content of this paper are prohibited.

5 Funding

This work was supported by the Natural Sciences and Engineering Research Council of Canada (Discovery Grant and Research Tools and Instruments programs).

6 Acknowledgments

The authors thank D. Sukachev for their input.

7 Disclosures

The authors have no competing interests to declare.

8 Data Availability Statement

Data underlying the results presented in this paper are not publicly available at this time but may be obtained from the authors upon reasonable request.

References

- [1] A Borghesi and G Guizzetti. Gallium phosphide (gap). In *Handbook of Optical Constants of Solids*, pages 445–464. Elsevier, 1997.
- [2] Matthew Gregory Borselli. *High-Q microresonators as lasing elements for silicon photonics*. PhD thesis, California Institute of Technology, 2006.
- [3] Robert W. Boyd. *Nonlinear optics*. Academic Press, 3 edition, 2008.
- [4] Alexander W Bruch, Xianwen Liu, Xiang Guo, Joshua B Surya, Zheng Gong, Liang Zhang, Junxi Wang, Jianchang Yan, and Hong X Tang. 17 000%/w second-harmonic conversion efficiency in single-crystalline aluminum nitride microresonators. *Applied Physics Letters*, 113(13):131102, 2018.
- [5] Tal Carmon, Lan Yang, and Kerry J. Vahala. Dynamical thermal behavior and thermal self-stability of microcavities. *Opt. Express*, 12(20):4742–4750, Oct 2004.
- [6] JU Furst, DV Strekalov, Dominique Elser, Mikael Lassen, Ulrik Lund Andersen, Christoph Marquardt, and Gerd Leuchs. Naturally phase-matched second-harmonic generation in a whispering-gallery-mode resonator. *Physical review letters*, 104(15):153901, 2010.
- [7] Zheng Gong, Xianwen Liu, Yuntao Xu, and Hong X Tang. Near-octave lithium niobate soliton microcomb. *Optica*, 7(10):1275–1278, 2020.
- [8] Zheng Gong, Xianwen Liu, Yuntao Xu, Mingrui Xu, Joshua B Surya, Juanjuan Lu, Alexander Bruch, Changling Zou, and Hong X Tang. Soliton microcomb generation at 2 μm in z-cut

- lithium niobate microring resonators. *Optics letters*, 44(12):3182–3185, 2019.
- [9] Zhenzhong Hao, Jie Wang, Shuqiong Ma, Wenbo Mao, Fang Bo, Feng Gao, Guoquan Zhang, and Jingjun Xu. Sum-frequency generation in on-chip lithium niobate microdisk resonators. *Photonics Research*, 5(6):623–628, 2017.
- [10] Hermann A. Haus. *Waves and Fields in Optoelectronics*. Prentice-Hall, Inc., 1984.
- [11] Yang He, Qi-Fan Yang, Jingwei Ling, Rui Luo, Hanxiao Liang, Mingxiao Li, Boqiang Shen, Heming Wang, Kerry Vahala, and Qiang Lin. Self-starting bi-chromatic linbo3 soliton microcomb. *Optica*, 6(9):1138–1144, Sep 2019.
- [12] Simon Hönl, Herwig Hahn, Yannick Baumgartner, Lukas Czornomaz, and Paul Seidler. Highly selective dry etching of gap in the presence of alxga1-xp with a sic4/sf6 plasma. *Journal of Physics D: Applied Physics*, 51(18):185203, 2018.
- [13] Bin-Lin Hu, Jing Zhang, Kai-Qin Cao, Shi-Jing Hao, De-Xin Sun, and Yin-Nian Liu. Research on the etalon effect in dispersive hyperspectral vnir imagers using back-illuminated ccds. *IEEE Transactions on Geoscience and Remote Sensing*, 56(9):5481–5494, 2018.
- [14] John David Jackson. *Classical Electrodynamics*. Wiley, 3 edition, 2001.
- [15] John D. Joannopoulos, Steven G. Johnson, Joshua N. Winn, and Robert D. Meade. *Photonic Crystals: Molding the Flow of Light*. Princeton University Press, 2 edition, 2008.
- [16] Hojoong Jung, Chi Xiong, King Y Fong, Xufeng Zhang, and Hong X Tang. Optical frequency comb generation from aluminum nitride microring resonator. *Optics letters*, 38(15):2810–2813, 2013.
- [17] L Koehler, P Chevalier, E Shim, B Desiatov, A Shams-Ansari, M Piccardo, Y Okawachi, M Yu, M Loncar, M Lipson, et al. Direct thermo-optical tuning of silicon microresonators for the mid-infrared. *Optics express*, 26(26):34965–34976, 2018.
- [18] Sergey Kruk, Alexander Poddubny, Daria Smirnova, Lei Wang, Alexey Slobozhanyuk, Alexander Shorokhov, Ivan Kravchenko, Barry Luther-Davies, and Yuri Kivshar. Nonlinear light generation in topological nanostructures. *Nature nanotechnology*, 14(2):126–130, 2019.
- [19] Paulina S Kuo, Jorge Bravo-Abad, and Glenn S Solomon. Second-harmonic generation using-quasi-phasematching in a gaas whispering-gallery-mode microcavity. *Nature communications*, 5(1):1–7, 2014.
- [20] Paulina S Kuo and Glenn S Solomon. On-and off-resonance second-harmonic generation in gaas microdisks. *Optics express*, 19(18):16898–16918, 2011.
- [21] David Lake. Multimode-optomechanics, spin-optomechanics, and nonlinear optics in photonic devices, 2020.
- [22] David P. Lake, Matthew Mitchell, Harishankar Jayakumar, Laís Fujii dos Santos, Davor Curic, and Paul E. Barclay. Efficient telecom to visible wavelength conversion in doubly resonant gallium phosphide microdisks. *Applied Physics Letters*, 108(3):031109, 2016.
- [23] Jacob S Levy, Mark A Foster, Alexander L Gaeta, and Michal Lipson. Harmonic generation in silicon nitride ring resonators. *Optics express*, 19(12):11415–11421, 2011.
- [24] Ming Li, Chang-Ling Zou, Chun-Hua Dong, and Dao-Xin Dai. Optimal third-harmonic generation in an optical microcavity with $\chi(2)$ and $\chi(3)$ nonlinearities. *Optics express*, 26(21):27294–27304, 2018.
- [25] Yihang Li, Xuefeng Jiang, Guangming Zhao, and Lan Yang. Whispering gallery mode microresonator for nonlinear optics, 2018.

- [26] Jintian Lin, Ni Yao, Zhenzhong Hao, Jianhao Zhang, Wenbo Mao, Min Wang, Wei Chu, Rongbo Wu, Zhiwei Fang, Lingling Qiao, Wei Fang, Fang Bo, and Ya Cheng. Broadband quasi-phase-matched harmonic generation in an on-chip monocrystalline lithium niobate microdisk resonator. *Phys. Rev. Lett.*, 122:173903, May 2019.
- [27] Shijie Liu, Yuanlin Zheng, and Xianfeng Chen. Cascading second-order nonlinear processes in a lithium niobate-on-insulator microdisk. *Optics letters*, 42(18):3626–3629, 2017.
- [28] Alan D Logan, Michael Gould, Emma R Schmidgall, Karine Hestroffer, Zin Lin, Weiliang Jin, Arka Majumdar, Fariba Hatami, Alejandro W Rodriguez, and Kai-Mei C Fu. 400%/w second harmonic conversion efficiency in 14 μm -diameter gallium phosphide-on-oxide resonators. *Optics express*, 26(26):33687–33699, 2018.
- [29] Alejandro Lorenzo-Ruiz and Yoan Léger. Generalization of second-order quasi-phase matching in whispering gallery mode resonators using berry phase. *ACS Photonics*, 7(7):1617–1621, 2020.
- [30] Juanjuan Lu, Joshua B. Surya, Xianwen Liu, Alexander W. Bruch, Zheng Gong, Yuntao Xu, and Hong X. Tang. Periodically poled thin-film lithium niobate microring resonators with a second-harmonic generation efficiency of 250,000%/w. *Optica*, 6(12):1455–1460, Dec 2019.
- [31] Rui Luo, Haowei Jiang, Steven Rogers, Hanxiao Liang, Yang He, and Qiang Lin. On-chip second-harmonic generation and broadband parametric down-conversion in a lithium niobate microresonator. *Opt. Express*, 25(20):24531–24539, Oct 2017.
- [32] Matthew Mitchell. Coherent cavity optomechanics in wide-band gap materials, 2019.
- [33] Matthew Mitchell, Aaron C. Hryciw, and Paul E. Barclay. Cavity optomechanics in gallium phosphide microdisks. *Applied Physics Letters*, 104(14):141104, 2014.
- [34] Mohamed Sabry Mohamed, Angelica Simbula, Jean-François Carlin, Momchil Minkov, Dario Gerace, Vincenzo Savona, Nicolas Grandjean, Matteo Galli, and Romuald Houdré. Efficient continuous-wave nonlinear frequency conversion in high-q gallium nitride photonic crystal cavities on silicon. *APL Photonics*, 2(3):031301, 2017.
- [35] Jeremy Moore, J Kenneth Douglas, Ian W Frank, Thomas A Friedmann, Ryan M Camacho, and Matt Eichenfield. Efficient second harmonic generation in lithium niobate on insulator. In *2016 Conference on Lasers and Electro-Optics (CLEO)*, pages 1–2. IEEE, 2016.
- [36] Jan Niehusmann, Andreas Vörckel, Peter Haring Bolivar, Thorsten Wahlbrink, Wolfgang Henschel, and Heinrich Kurz. Ultrahigh-quality-factor silicon-on-insulator microring resonator. *Opt. Lett.*, 29(24):2861–2863, Dec 2004.
- [37] Yoshitomo Okawachi, Kasturi Saha, Jacob S Levy, Y Henry Wen, Michal Lipson, and Alexander L Gaeta. Octave-spanning frequency comb generation in a silicon nitride chip. *Optics letters*, 36(17):3398–3400, 2011.
- [38] Ardavan F. Oskooi, David Roundy, Mihai Ibanescu, Peter Bermel, J.D. Joannopoulos, and Steven G. Johnson. Meep: A flexible free-software package for electromagnetic simulations by the fdtd method. *Computer Physics Communications*, 181(3):687 – 702, 2010.
- [39] DF Parsons and PD Coleman. Far infrared optical constants of gallium phosphide. *Applied optics*, 10(7):1683_1–1685, 1971.
- [40] WHP Pernice, C Xiong, C Schuck, and HX Tang. Second harmonic generation in phase matched aluminum nitride waveguides and micro-ring resonators. *Applied Physics Letters*, 100(22):223501, 2012.

- [41] Martin H. P. Pfeiffer, Clemens Herkommer, Jun-qi Liu, Hairun Guo, Maxim Karpov, Erwan Lucas, Michael Zervas, and Tobias J. Kippenberg. Octave-spanning dissipative kerr soliton frequency combs in si₃n₄ microresonators. *Optica*, 4(7):684–691, Jul 2017.
- [42] Kelley Rivoire, Sonia Buckley, Fariba Hatami, and Jelena Vučković. Second harmonic generation in gap photonic crystal waveguides. *Applied Physics Letters*, 98(26):263113, 2011.
- [43] Kelley Rivoire, Ziliang Lin, Fariba Hatami, W. Ted Masselink, and Jelena Vučković. Second harmonic generation in gallium phosphide photonic crystal nanocavities with ultralow continuous wave pump power. *Opt. Express*, 17(25):22609–22615, Dec 2009.
- [44] Kelley Rivoire, Ziliang Lin, Fariba Hatami, and Jelena Vučković. Sum-frequency generation in doubly resonant gap photonic crystal nanocavities. *Applied Physics Letters*, 97(4):043103, 2010.
- [45] Alejandro Rodriguez, Marin Soljačić, J. D. Joannopoulos, and Steven G. Johnson. $\chi(2)$ and $\chi(3)$ harmonic generation at a critical power in inhomogeneous doubly resonant cavities. *Opt. Express*, 15(12):7303–7318, Jun ts.
- [46] Iannis Roland, Maksym Gromovyi, Yijia Zeng, Moustafa El Kurdi, Sebastien Sauvage, Christelle Brimont, Thierry Guillet, Bruno Gayral, Fabrice Semond, Jean-Yves Duboz, et al. Phase-matched second harmonic generation with on-chip gan-on-si microdisks. *Scientific reports*, 6:34191, 2016.
- [47] Kiyotaka Sasagawa and Masahiro Tsuchiya. Highly efficient third harmonic generation in a periodically poled mgo: Linbo₃ disk resonator. *Applied Physics Express*, 2(12):122401, 2009.
- [48] Katharina Schneider, Pol Welter, Yannick Baumgartner, Herwig Hahn, Lukas Czornomaz, and Paul Seidler. Gallium phosphide-on-silicon dioxide photonic devices. *Journal of Lightwave Technology*, 36(14):2994–3002, Jul 2018.
- [49] Daria Smirnova, Sergey Kruk, Daniel Leykam, Elizaveta Melik-Gaykazyan, Duk-Yong Choi, and Yuri Kivshar. Third-harmonic generation in photonic topological metasurfaces. *Physical review letters*, 123(10):103901, 2019.
- [50] S. M. Spillane, T. J. Kippenberg, O. J. Painter, and K. J. Vahala. Ideality in a fiber-taper-coupled microresonator system for application to cavity quantum electrodynamics. *Phys. Rev. Lett.*, 91:043902, Jul 2003.
- [51] Joshua B Surya, Xiang Guo, Chang-Ling Zou, and Hong X Tang. Efficient third-harmonic generation in composite aluminum nitride/silicon nitride microrings. *Optica*, 5(2):103–108, 2018.
- [52] Lillian Thiel, Alan D. Logan, Srivatsa Chakravarthi, Shivangee Shree, Karine Hestroffer, Fariba Hatami, and Kai-Mei C. Fu. Target-wavelength-trimmed second harmonic generation with gallium phosphide-on-nitride ring resonators, 2021.
- [53] Akira Tomita and Raymond Y. Chiao. Observation of berry’s topological phase by use of an optical fiber. *Phys. Rev. Lett.*, 57:937–940, Aug 1986.
- [54] You Wang, Li-Jun Lang, Ching Hua Lee, Baile Zhang, and YD Chong. Topologically enhanced harmonic generation in a nonlinear transmission line metamaterial. *Nature communications*, 10(1):1–7, 2019.
- [55] Dalziel J. Wilson, Katharina Schneider, Simon Hönl, Miles Anderson, Yannick Baumgartner, Lukas Czornomaz, Tobias J. Kippenberg, and Paul Seidler. Integrated gallium phosphide nonlinear photonics. *Nature Photonics*, 14(1):57–62, Jan 2020.
- [56] Marcelo Wu, Aaron C. Hryciw, Chris Healey, David P. Lake, Harishankar Jayakumar, Mark R. Freeman, John P. Davis, and Paul E. Barclay. Dissipative and dispersive optomechanics in a nanocavity torque sensor. *Phys. Rev. X*, 4:021052, Jun 2014.

- [57] Amnon Yariv and Pochi Yeh. *Photonics: Optical Electronics in Modern Communications*. Oxford Univ. Press, 6 edition, 2007.
- [58] Xiaona Ye, Shijie Liu, Yuping Chen, Yuanlin Zheng, and Xianfeng Chen. Sum-frequency generation in lithium-niobate-on-insulator microdisk via modal phase matching. *Optics Letters*, 45(2):523–526, 2020.
- [59] Rong Yu, Chunling Ding, Jiangpeng Wang, and Duo Zhang. Enhanced visible light generation in an active microcavity via third-harmonic conversion beyond the non-depletion approximation. *Journal of Applied Physics*, 122(24):244303, 2017.